Available online at www.sciencedirect.com
ScienceDirect
Physics of the Earth and Planetary Interiors 166 (2008) 226–238
PHYSICS OF THE EARTH AND PLANETARY INTERIORS
www.elsevier.com/locate/pepi

Geomagnetic dipole tilt changes induced by core flow

Hagay Amit [a,*], Peter Olson [b]

[a] *Equipe de Géomagnétisme, Institut de Physique du Globe de Paris (Institut de Recherche associé au CNRS et à l'Université Paris 7), 4 Place Jussieu, 75252 Paris Cedex 05, France*

[b] *Department of Earth and Planetary Sciences, Johns Hopkins University, Baltimore, MD 21218, USA*

Received 20 April 2007; received in revised form 26 October 2007; accepted 22 January 2008

Abstract

The tilt of the geomagnetic dipole decreased from about 11.7° in 1960 to 10.5° in 2005, following more than a century when it remained nearly constant. The recent poleward motion of the dipole axis is primarily due to a rapid decrease in the equatorial component of the dipole moment vector. Using maps of the equatorial dipole moment density and its secular change derived from core field models, we identify regions on the core–mantle boundary where the present-day tilt decrease is concentrated. Among the possible causes of equatorial dipole moment change on the core–mantle boundary, tangential magnetic diffusion is negligible on these time scales, and although radial magnetic diffusion is potentially significant, the rapid changes in equatorial moment density indicate it is not the dominant mechanism. We show that magnetic flux transport can account for most of the observed equatorial dipole moment change. Frozen-flux core flow models derived from geomagnetic secular variation reveal a nearly balanced pattern of advective sources and sinks for the equatorial dipole moment below the core–mantle boundary. The recent tilt decrease originates from two advective sinks, one beneath Africa where positive radial magnetic field is transported westward away from the equatorial dipole axis, the other beneath North America where negative radial magnetic field is transported northward away from the equatorial dipole axis. Each of these sinks is related to a prominent gyre that has evolved significantly over the past few decades, indicating the strong variability of the large-scale circulation in the outer core on this time scale.

Keywords: Geomagnetic field; Geomagnetic dipole tilt; Equatorial dipole moment; Core flow; Advective sources; Geodynamo

1. Introduction

The geomagnetic field contains a broad spectrum of spherical harmonic components, but the dipole part of the field is particularly important in the geodynamo because it represents the largest scale and most persistent electric current system in the Earth's core. The dipole part dominates the other spherical harmonics in the present-day field at the Earth's surface and to a lesser extent at the core–mantle boundary (CMB), and the tilt of the dipole is the primary large-scale deviation in the field from axial symmetry (Jackson et al., 2000; Mcmillan and Maus, 2005; Olsen et al., 2006). The dipole field also has far longer time constants than the other harmonics, so the geomagnetic field becomes increasingly dipolar with longer time averages (Carlut et al., 2000; Korte and Constable, 2005). However the time constant of the equatorial component of the dipole is shorter than the time constant of its axial component (Hongre et al., 1998), so that with longer time averages the field also becomes increasingly axisymmetric (Merrill et al., 1998).

The dynamo mechanisms that make the time-average geomagnetic field axisymmetric are not clear. It is often supposed that the main symmetry-enhancing process consists of geomagnetic westward drift (Bullard et al., 1950; Yukutake, 1967; McFadden et al., 1985). Sustained westward drift caused by core flow or by westward propagating waves (Hide, 1966) would eventually suppress the dipole tilt and all other non-axisymmetric terms in the field, and also would induce a retrograde precession of the tilted dipole axis about the geographic pole. However, recent spherical harmonic models of the geomagnetic field structure over the past 7 kyr by Korte and Constable (2005) reveal a far more complex picture of the secular variation in general, and the dipole behavior in particular. As shown in Fig. 1, the motion of the north geomagnetic pole (NGP) in this model consists of a sequence off-axis loops and hairpin turns, and contains nearly as much north–south (meridional) motion as east–west (azimuthal) motion. Some of the NGP

* Corresponding author.
E-mail address: hagay@ipgp.jussieu.fr (H. Amit).

0031-9201/$ – see front matter © 2008 Elsevier B.V. All rights reserved.
doi:10.1016/j.pepi.2008.01.007

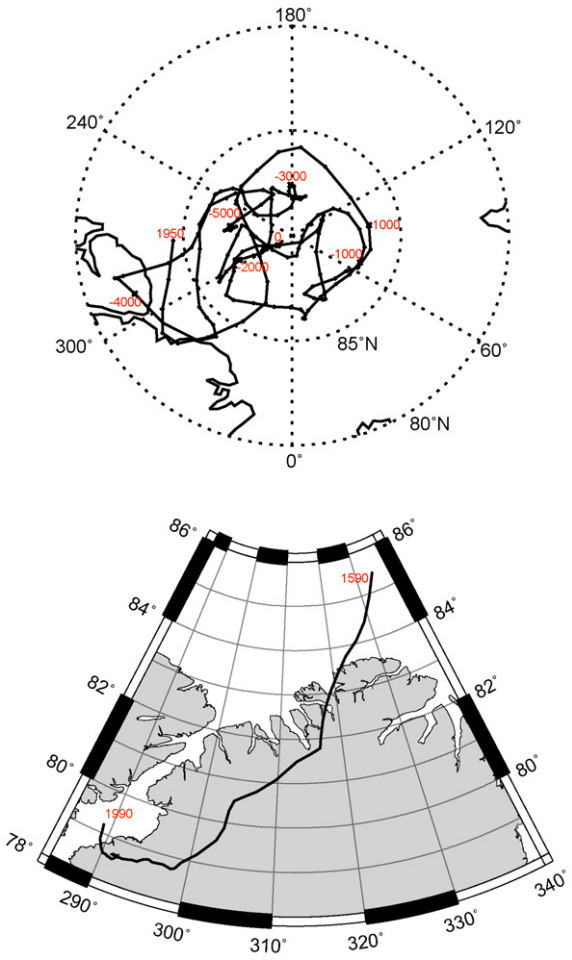

Fig. 1. Top: NGP motion in the last seven millenia according to the *CALS7K* archaemagnetic field model (Korte and Constable, 2005); bottom: NGP motion in the last four centuries according to the *gufm1* historical field model (Jackson et al., 2000).

loops are retrograde as expected for westward drift, but some are prograde, and most are not centered on the geographic pole. The NGP path in the historical field model of Jackson et al. (2000) in Fig. 1 also shows first-order departures from uniform westward drift, and actually contains more meridional motion of the geomagnetic pole than azimuthal motion over the past 400 years. The NGP motions in Fig. 1 are not consistent with westward drift acting alone, and indeed they are difficult to explain by any purely azimuthal motion. The large, irregular, and sometimes rapid tilt changes in Fig. 1 indicate that meridional motion of the dipole axis is just as important as its azimuthal motion in producing the time-average symmetric state.

Dipole tilt affects the structure and dynamics of the external field, including the location of magnetospheric cusps (Newell and Meng, 1989; Østgaard et al., 2007) and the field-aligned currents and Alfvén waves that power the auroral ovals (Keiling et al., 2003). In Earth's magnetosphere, the weak field region called the South Atlantic Anomaly is partly caused by the dipole tilt (Heirtzler, 2002). The Van Allen radiation belts, which consist of charged particles extracted from the solar wind, are inclined with respect to the rotation axis in proportion to the dipole tilt (Brasseur and Solomon, 1984).

Dipole tilt is not unique to the geomagnetic field. Among the other planets in the solar system, nearly all tilt angles are represented, ranging from nearly zero dipole tilt in Saturn (Smith et al., 1980), to 9.6° tilt in Jupiter (Smith et al., 1975), to large tilts of the dipolar components of the fields in Uranus and Neptune (Connerney et al., 1987, 1992). Both Saturn and Jupiter feature strong alternating zonal winds in their atmospheres, yet their magnetic fields, although both dipole-dominant, show very different amounts of tilt. In addition, there is evidence that the tilt of Jupiter's field changes on decadal time scales (Russell et al., 2001). Uranus and Neptune also have zonal wind patterns in their atmospheres, yet both magnetic fields lack the dipolar structure of fields in the gas giants.

The variety of dipole tilts among planetary magnetic fields with respect to their rotation axes is puzzling, because theory indicates that a planet's rotation should control the symmetry of its dynamo. Proposed explanations include differences in the geometry of the dynamo-producing regions in planetary interiors (Stanley and Bloxham, 2004; Heimpel et al., 2005), and dynamical variations between the planets, such as the relative strength of convection versus zonal flow (Stevenson, 1980) and the presence of stable stratification (Christensen, 2006). These effects might explain the differences between the planetary dipole tilts, but they do not offer much insight to the geomagnetic tilt changes. Several studies have identified magnetic flux transport in the core and flux expulsion through the CMB as the main mechanisms of geomagnetic dipole moment intensity decrease (e.g. Bloxham and Gubbins, 1985; Gubbins, 1987; Gubbins et al., 2006; Olson and Amit, 2006), but the processes that produce tilt changes, including reversals and excursions (Merrill and McFadden, 1999), are poorly understood.

In this paper we examine the causes of the historical geomagnetic dipole tilt change and their implications for the geodynamo. We develop a kinematic theory for dipole moment change in terms of tangential advection of radial magnetic field, radial magnetic diffusion and tangential magnetic diffusion processes just below the CMB. First we show that dipole tilt changes since 1840, including the rapid decrease event that commenced around 1960, are primarily due to changes in the equatorial component of the dipole moment. We then construct maps of the equatorial moment density and its secular change on the CMB. These maps indicate that magnetic diffusion in the outer core is unlikely the main cause of the observed tilt changes. Based on the kinematic theory and a frozen-flux model of core flow inferred from the secular variation of the core field, we construct maps of the advective sources and sinks of equatorial dipole moment on the CMB, and identify regions where magnetic field transport by the large-scale time-dependent core flow is inducing most of the tilt change.

2. Observed dipole tilt changes

According to the *gufm1* geomagnetic field model based on surface observatories and the Magsat 1980 satellite (Jackson et al., 2000) and more recent satellite-based models (Mcmillan and Maus, 2005; Olsen et al., 2006), the tilt of the geomagnetic dipole vector changed very little between 1840 and 1960. The

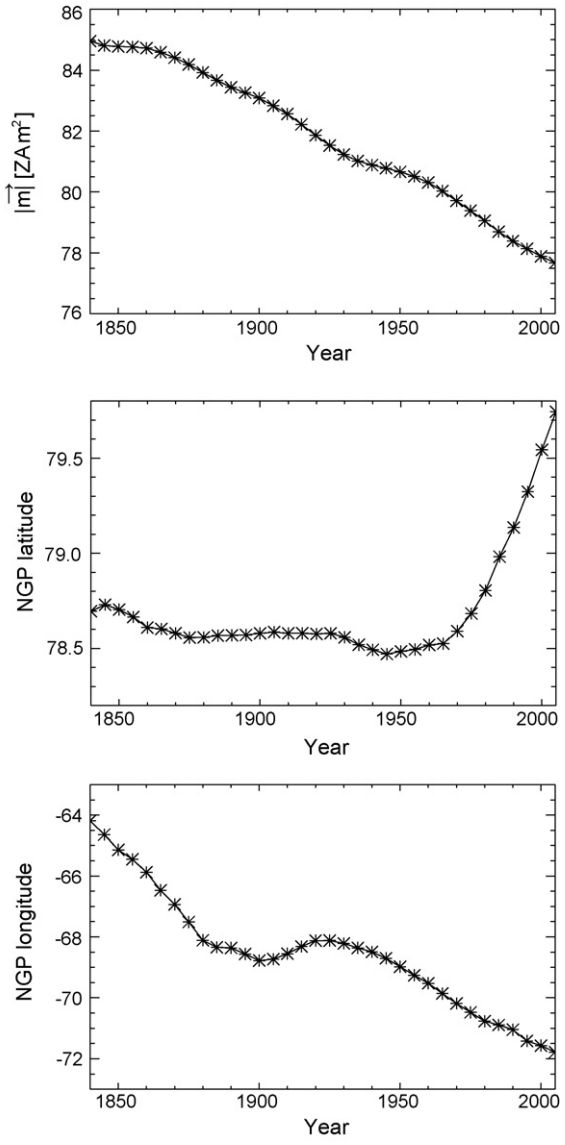

Fig. 2. Geomagnetic dipole moment intensity in Z A m^2 ($Z \equiv 10^{21}$) (top), NGP latitude (middle) and NGP longitude (bottom), 1840–2005. Data taken from the historical core field model *gufm1* for 1840–1990 (Jackson et al., 2000) and the 10th IGRF model for 1995–2005 (Mcmillan and Maus, 2005).

latitude of the north geomagnetic pole moved from 78.7°N in 1840 to 78.5°N in 1960, while its longitude moved generally westward with an average angular velocity of about 0.04° yr^{-1} over the same period (Fig. 2).

Since about 1960 the NGP has drifted rapidly northward, reaching 79.7°N in 2005. Both the axial and the equatorial components of the dipole moment are now decreasing rapidly, as are the dipole intensity and the tilt angle. The rates of decrease at 2005 were $\dot{m}_z = 0.72T$ A m^2 s^{-1}($T \equiv 10^{12}$) for the axial moment m_z and $\dot{m}_e = -1.96T$ A m^2 s^{-1} for the equatorial moment m_e, and the rate of tilt change at 2005 was $\dot{\theta}_0 = -0.05°$ yr^{-1}. The current tilt decrease event involves a 13.5% drop in the equatorial dipole moment since 1960. This is roughly 50 times the free decay rate of a fundamental-mode dipole field in the core and it has overwhelmed the better-known 3.0% drop in the axial component of the dipole moment over the same period of time, resulting in the 1.2° northward motion of the NGP.

3. Kinematic theory for dipole moment change

The dipole moment vector $\vec{m}$ due to a distributed electric current vector $\vec{J}$ is

$$\vec{m} = \frac{1}{2}\int_V \vec{r} \times \vec{J}\, \mathrm{d}V, \tag{1}$$

where $\vec{r}$ is the position vector and V is the volume of the conductor. The dipole moment vector can also be expressed in terms of the magnetic field $\vec{B}$ in the same volume as

$$\vec{m} = \frac{3}{2\mu_0}\int_V \vec{B}\, \mathrm{d}V, \tag{2}$$

where $\mu_0 = 4\pi \times 10^{-7}$ N A^{-2} is permeability of free space. The temporal rate of change of the dipole moment vector is therefore

$$\dot{\vec{m}} = \frac{3}{2\mu_0}\int_V \dot{\vec{B}}\, \mathrm{d}V. \tag{3}$$

Using Faraday's law, (3) can be rewritten as

$$\frac{2\mu_0}{3}\dot{\vec{m}} = -\int_V \nabla \times \vec{E}\, \mathrm{d}V = -\int_S \hat{r} \times \vec{E}\, \mathrm{d}S, \tag{4}$$

where $\vec{E}$ is the electric field, $\hat{r}$ the unit vector normal to the conductor boundary and S is the conductor surface. The electric field can be expressed in terms of the magnetic and velocity fields in the conductor using Ohm's law:

$$\vec{E} = -\vec{u} \times \vec{B} + \lambda \nabla \times \vec{B}, \tag{5}$$

where $\vec{u}$ is the velocity field and λ is the magnetic diffusivity. Substituting (5) into (4) and assuming the normal component of the velocity vanishes on approach to the conductor boundary gives the rate of change of the dipole moment vector in terms of the magnetic and velocity fields just below the boundary (Moffatt, 1978; Davidson, 2001):

$$\frac{2\mu_0}{3}\dot{\vec{m}} = \int_S \vec{u}(\vec{B}\cdot\hat{r})\, \mathrm{d}S - \lambda\int_S \hat{r} \times (\nabla \times \vec{B})\, \mathrm{d}S. \tag{6}$$

The geomagnetic dipole moment vector is generally expressed in terms of a component m_z parallel to the rotation axis and two components m_x and m_y in the equatorial plane:

$$\vec{m} = m_z\hat{z} + m_x\hat{x} + m_y\hat{y}. \tag{7}$$

The axial component of the dipole moment can be written as

$$m_z = \frac{4\pi a^3}{\mu_0} g_1^0 = \int_S \rho_z\, \mathrm{d}S. \tag{8}$$

in terms of the axial dipole moment density ρ_z on the CMB:

$$\rho_z = \frac{3r_c}{2\mu_0} B_r \cos\theta, \tag{9}$$

where a is the radius of the Earth, r_c the radius of the core, g_1^0 the axial dipole Gauss coefficient and B_r is the radial component of $\vec{B}$ in a spherical coordinate system (ϕ, θ, r). From the axial

component of (6), the rate of change of the axial dipole moment can be written as

$$\dot{m}_z = \int_S \dot{\rho}_z \, \mathrm{d}S = \frac{3}{2\mu_0} \int_S [A_z + D_{\mathrm{r}z} + D_{\mathrm{t}z}] \, \mathrm{d}S, \tag{10}$$

where

$$A_z = -u_\theta \sin\theta \, B_\mathrm{r} \tag{11}$$

is the contribution from meridional advection. The contributions from radial and tangential magnetic diffusion to axial dipole change, as well as diffusive contributions to the other dipole components changes, are given in Appendix A.

Density functions can also be defined for the dipole moment components along the Cartesian x and y coordinates in the equatorial plane. The dipole moment densities along longitudes 0°E and 90°E, respectively are

$$\rho_x = \frac{3r_\mathrm{c}}{2\mu_0} B_\mathrm{r} \sin\theta \cos\phi, \tag{12}$$

$$\rho_y = \frac{3r_\mathrm{c}}{2\mu_0} B_\mathrm{r} \sin\theta \sin\phi, \tag{13}$$

and the corresponding dipole moment components are

$$m_x = \frac{4\pi a^3}{\mu_0} g_1^1 = \int_S \rho_x \, \mathrm{d}S, \tag{14}$$

$$m_y = \frac{4\pi a^3}{\mu_0} h_1^1 = \int_S \rho_y \, \mathrm{d}S, \tag{15}$$

where g_1^1 and h_1^1 are the equatorial dipole Gauss coefficients. From the x component of (6), the rate of change of m_x is

$$\dot{m}_x = \frac{3}{2\mu_0} \int_S [A_x + D_{\mathrm{r}x} + D_{\mathrm{t}x}] \, \mathrm{d}S, \tag{16}$$

where the contribution by tangential advection is

$$A_x = (u_\theta \cos\theta \cos\phi - u_\phi \sin\phi) B_\mathrm{r}. \tag{17}$$

Similarly, the y component of (6) yields a corresponding expression for the rate of change of m_y:

$$\dot{m}_y = \frac{3}{2\mu_0} \int_S [A_y + D_{\mathrm{r}y} + D_{\mathrm{t}y}] \, \mathrm{d}S \tag{18}$$

with the advective contribution being

$$A_y = (u_\theta \cos\theta \sin\phi + u_\phi \cos\phi) B_\mathrm{r}. \tag{19}$$

In terms of m_x and m_y, the longitude of the dipole is

$$\phi_0 = \tan^{-1}\left(\frac{m_y}{m_x}\right) = \tan^{-1}\left(\frac{h_1^1}{g_1^1}\right) \tag{20}$$

and the azimuthal angular velocity of the dipole axis is

$$\dot{\phi}_0 = \frac{\dot{m}_y m_x - \dot{m}_x m_y}{{m_x}^2 + {m_y}^2} = \frac{\dot{h}_1^1 g_1^1 - \dot{g}_1^1 h_1^1}{{g_1^1}^2 + {h_1^1}^2}. \tag{21}$$

We now define the equatorial component of the dipole moment as

$$m_\mathrm{e} = \frac{4\pi a^3}{\mu_0} \sqrt{{g_1^1}^2 + {h_1^1}^2} = \int_S \rho_\mathrm{e} \, \mathrm{d}S \tag{22}$$

in terms of the equatorial dipole moment density ρ_e on the CMB:

$$\rho_\mathrm{e} = \frac{3r_\mathrm{c}}{2\mu_0} B_\mathrm{r} \sin\theta \cos\phi', \tag{23}$$

where $\phi' = \phi - \phi_0$ is the longitude relative to the magnetic pole and $\phi_0(t)$ is the time-dependent longitude of the magnetic pole. The equatorial component of (6) yields an expression for the rate of change of the equatorial dipole moment in terms of three contributions:

$$\dot{m}_\mathrm{e} = \frac{3}{2\mu_0} \int_S [A_\mathrm{e} + D_\mathrm{re} + D_\mathrm{te}] \, \mathrm{d}S. \tag{24}$$

Note that the equatorial unit vector $\hat{e}$ is time-dependent, therefore in general, $\hat{e} \cdot \dot{\vec{m}} = \dot{m}_\mathrm{e} - \vec{m} \cdot \dot{\hat{e}}$, but since $\vec{m} \cdot \dot{\hat{e}} = 0$, we obtain (24). The contribution to $\dot{m}_\mathrm{e}$ from tangential advection is

$$A_\mathrm{e} = (u_\theta \cos\theta \cos\phi' - u_\phi \sin\phi') B_\mathrm{r}. \tag{25}$$

The magnitude of the dipole moment vector is in terms of the axial and equatorial dipole moment components:

$$|\vec{m}| = \sqrt{m_z^2 + m_\mathrm{e}^2} = \frac{4\pi a^3}{\mu_0} g_1, \tag{26}$$

where $g_1 \equiv \sqrt{{g_1^0}^2 + {g_1^1}^2 + {h_1^1}^2}$. Its rate of change is therefore

$$|\dot{\vec{m}}| = \frac{m_z \dot{m}_z + m_\mathrm{e} \dot{m}_\mathrm{e}}{|\vec{m}|} = \frac{4\pi a^3}{\mu_0} \frac{g_1^0 \dot{g}_1^0 + g_1^1 \dot{g}_1^1 + h_1^1 \dot{h}_1^1}{g_1}. \tag{27}$$

The dipole tilt angle θ_0 can also be written in terms of the axial and equatorial dipole moment components:

$$\theta_0 = \tan^{-1}\left(\frac{m_\mathrm{e}}{m_z}\right) = \tan^{-1}\left(\frac{\sqrt{{g_1^1}^2 + {h_1^1}^2}}{g_1^0}\right), \tag{28}$$

so its rate of change is

$$\dot{\theta}_0 = \frac{\dot{m}_\mathrm{e} m_z - \dot{m}_z m_\mathrm{e}}{|\vec{m}|^2} = \frac{(g_1^1 \dot{g}_1^1 + h_1^1 \dot{h}_1^1) g_1^0 - ({g_1^1}^2 + {h_1^1}^2) \dot{g}_1^0}{g_1^2 \sqrt{{g_1^1}^2 + {h_1^1}^2}}. \tag{29}$$

Note that because the current geomagnetic polarity is positive in the southern hemisphere, the positive dipole axis is in the southern hemisphere, for example (108.2°E, 79.7°S) in 2005. The NGP is the location of the tail of the dipole moment vector, so $\phi_\mathrm{ngp} = \phi_0 - \pi$ and $\theta_\mathrm{ngp} = \pi - \theta_0$. We refer to the tilt angle as the absolute latitudinal distance between the geographic north pole and the NGP.

3.1. Alternative approach

We have adopted a fundamental approach starting from the pre-Maxwell equations to derive an equation for the secular variation of the dipole moment vector (Moffatt, 1978; Davidson,

2001), from which we extracted the equations for the rates of change of the various components of the dipole moment. It is also possible to obtain the same equations using a different approach, perhaps more intuitive, directly from the radial magnetic induction equation just below the CMB:

$$\dot{B}_r = -\nabla_h \cdot (\vec{u}_h B_r) + \lambda \left(\frac{1}{r_c} \frac{\partial^2}{\partial r^2} (r^2 B_r) + \nabla_h^2 B_r \right). \quad (30)$$

For example, to get the equation for the rate of change of the axial dipole, we multiply (30) by $(3r_c/2\mu_0)\cos\theta$ and integrate over the CMB surface. The first term on the left hand side becomes

$$\frac{3r_c}{2\mu_0} \int_S \dot{B}_r \cos\theta \, dS = \frac{3r_c}{2\mu_0} \frac{\partial}{\partial t} \int_S B_r \cos\theta \, dS = \dot{m}_z. \quad (31)$$

The first term on the right hand side of (30) becomes, using the chain rule:

$$-\frac{3r_c}{2\mu_0} \int_S \nabla_h \cdot (\vec{u}_h B_r) \cos\theta \, dS$$
$$= -\frac{3r_c}{2\mu_0} \int_S (\nabla_h \cdot (\vec{u}_h B_r \sin\theta) - B_r \vec{u}_h \cdot \nabla \cos\theta) \, dS. \quad (32)$$

The first term on the right hand side of (32) is a closed surface integral of a surface divergence field and is identically zero according to the divergence theorem. Since $\vec{u}_h \cdot \nabla \cos\theta = -(\sin\theta/r_c)u_\theta$, (32) becomes

$$-\frac{3r_c}{2\mu_0} \int_S \nabla_h \cdot (\vec{u}_h B_r) \cos\theta \, dS = -\frac{3}{2\mu_0} \int_S u_\theta \sin\theta \, B_r \, dS. \quad (33)$$

From the balance of (31) and (33) it is clear that the advective contribution to axial dipole change is identical to (11). The same approach can be used to derive the diffusive contributions, as well the three contributions to the other dipole components rates of change.

4. Equatorial dipole moment density on the core–mantle boundary

The geomagnetic tilt depends on the magnitudes of both the axial and equatorial dipole moment components according to (28). However, because $m_z \gg m_e$ throughout the historical record, changes in dipole moment intensity (27) are mostly due to changes in m_z (Gubbins, 1987; Gubbins et al., 2006; Olson and Amit, 2006), whereas changes in dipole tilt (29) are mostly associated with changes in the equatorial dipole moment m_e. This relationship is evident in Fig. 3, where both m_e and θ_0 follow very similar trends since 1840, including the nearly constant period until 1960 and the ensuing rapid decrease event.

Fig. 4 shows maps of the geomagnetic field on the CMB at epochs 1860, 1900, 1940 and 1980, obtained from the historical core field model *gufm1* (Jackson et al., 2000). These epochs were selected because they span the historical period while avoiding the endpoints of the field model. The three earlier maps are at epochs when the tilt was nearly constant, whereas the last map is during the recent rapid tilt decrease event. The left column of maps in Fig. 4 shows the radial component of the field B_r, the right column shows the equatorial dipole moment density ρ_e as defined by (23).

Large contributions to the axial moment m_z come from the high-intensity, high-latitude prominent B_r patches in Fig. 4 (Gubbins and Bloxham, 1987; Bloxham, 2002). The historical decrease of the axial dipole moment is due to weakening and equatorward motion of these high-intensity field lobes, combined with expansion and intensification of the regions with reversed B_r (Gubbins et al., 2006; Olson and Amit, 2006), which are seen in Fig. 4 beneath the South Atlantic and the southern portion of South America. There a strong positive B_r lobe has been progressively replaced by a spot with negative B_r. Below the Indian Ocean, a strong positive B_r lobe has moved equatorward, also reducing the axial dipole.

In contrast to the axial moment density, the equatorial moment density ρ_e in Fig. 4 shows a four-quadrant (spherical harmonic Y_2^1-type) structure. The quadrant boundaries that partition ρ_e are approximately the equator and the two meridians located 90° east and west, respectively, from ϕ_0. Defined this way, the NW and SE quadrants of ρ_e make positive contributions to m_e throughout the historical record, whereas the NE and SW quadrants make negative contributions. There is tendency in the ρ_e maps for cancellation between north–south and east–west pairs of quadrants, a consequence of the dominance of the axial dipole in the core field. However, these cancellations are not complete. The positive contributions from the NW and SE quadrants outweigh the negative contributions from the NE and SW quadrants at all times in the historical record. The smallest contribution in Fig. 4 comes from the SW quadrant. The positive

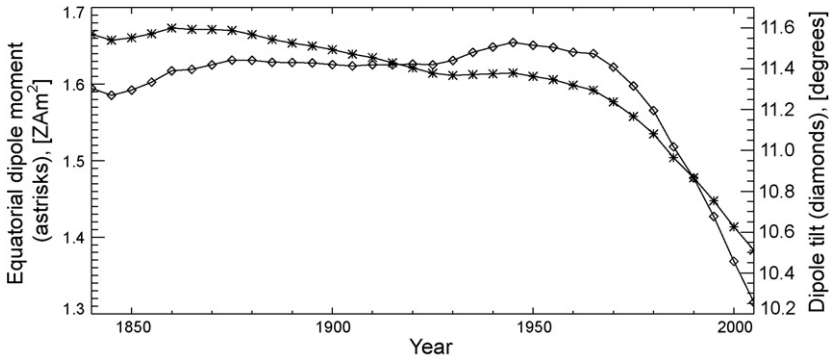

Fig. 3. Equatorial dipole moment in Z A m^2 (asterisks, left Y-axis) and dipole tilt in degrees (diamonds, right Y-axis), 1840–2005. Data sources as in Fig. 2.

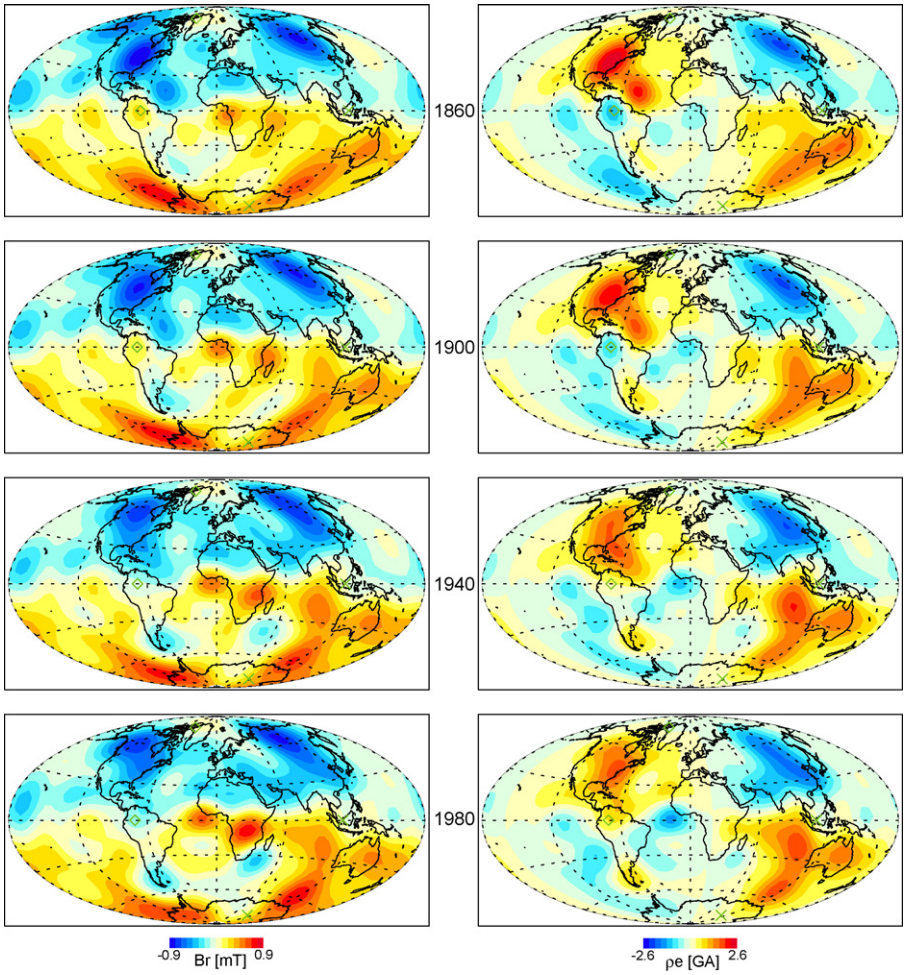

Fig. 4. Radial magnetic field in mT (left) and equatorial dipole moment density in G A ($G \equiv 10^9$) (right) based on *gufm1* for 1860, 1900, 1940 and 1980. Xs (green in web version) represent pole location and its equatorial projection, diamonds (green in web version) represent antipole location and its equatorial projection.

density in this quadrant is mostly a product of the large reversed flux patch below Patagonia seen in the B_r maps. The largest contribution to ρ_e comes from the SE quadrant. Accordingly, it is the imbalance between eastern and western quadrants in the southern hemisphere that is largely responsible for the magnitude of the equatorial dipole moment, and hence the magnitude of the tilt. This same imbalance between southern hemisphere quadrants likewise controls the longitude of the equatorial dipole moment vector.

Fig. 5 shows the secular variation of the radial field $\dot{B}_r$ (left) and the secular variation of the equatorial moment density $\dot{\rho}_e$ (right) on the CMB at the same epochs shown in Fig. 4. It is perhaps surprising that $\dot{\rho}_e$ appears to be nearly balanced, even at 1980 during the rapid tilt decrease event. If instead of being nearly balanced, $\dot{\rho}_e$ were equal its minimum value in Fig. 5 over the entire CMB, then m_e would be decreasing at about 80 times faster than its decrease rate in 2005 (about 2300 times its free decay rate) and the tilt would be decreasing by nearly $4^\circ\,\mathrm{yr}^{-1}$.

Another important property of $\dot{\rho}_e$ is its variability in time. Only a small tilt change occurred between 1840 and 1960, yet even the earlier three $\dot{\rho}_e$ maps that sample this period show very different morphologies. The speed at which new structures form is illustrated by the emergence of negative $\dot{\rho}_e$ spots below Bermuda, the equatorial Atlantic and Southeast Asia. These structures become particularly prominent in the 1980 map. These regions also display strong signatures in $\dot{B}_r$, with diminished negative field beneath Bermuda, enhanced and westward motion of positive field beneath the equatorial Atlantic, and southward motion of the magnetic equator beneath Southeast Asia. In the next section we show that this variability can be explained by frozen-flux transport by large-scale core flow.

5. Equatorial dipole moment change mechanisms

5.1. Diffusive mechanisms

The contributions from the three kinematic mechanisms responsible for the tilt change can be obtained by analyzing the terms in the equatorial dipole moment equation (24). At the scales of the core field shown in Fig. 4, the contribution from tangential diffusion D_{te} is numerically smaller than $\dot{\rho}_e$ by nearly two orders of magnitude, for any plausible core magnetic diffusivity λ. Accordingly, the tangential magnetic diffusion term can be safely ignored.

In contrast, the radial diffusion term D_{re} is certainly significant in the magnetic boundary layer below the CMB, and

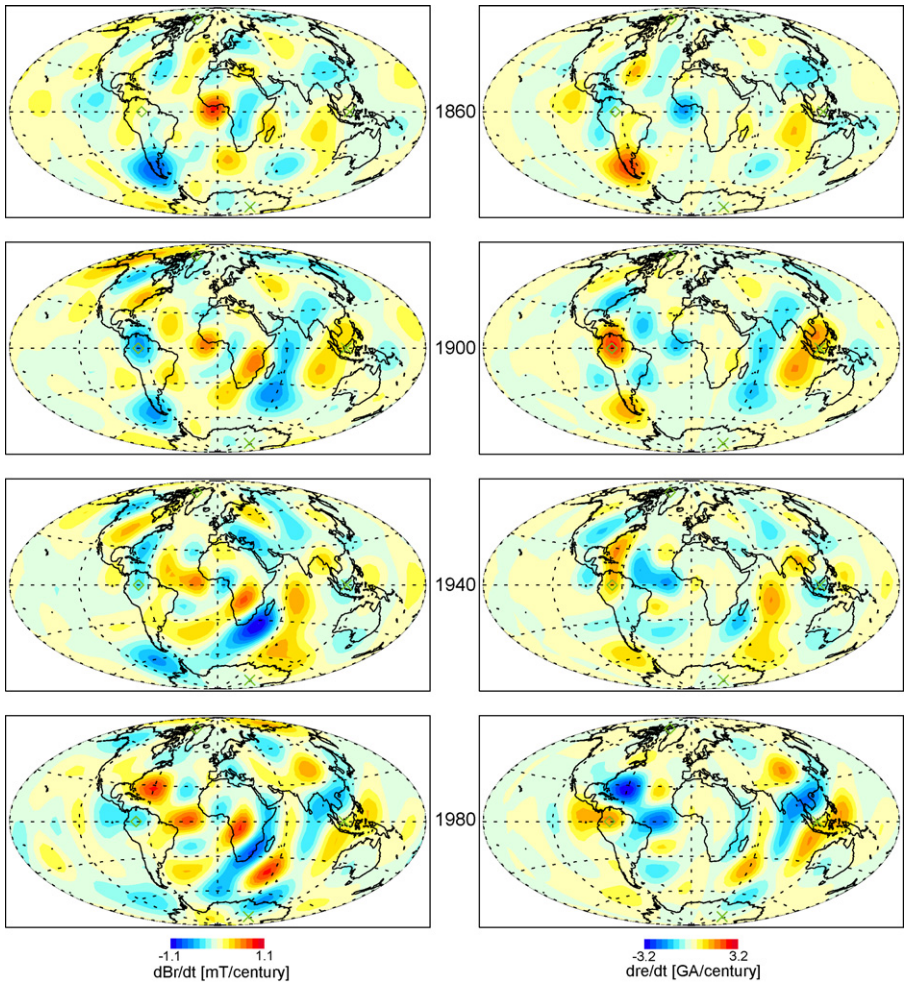

Fig. 5. Secular variation of the radial magnetic field in mT/century (left) and secular variation of the equatorial dipole moment density in *G* A/century (right) based on *gufm1* for 1860, 1900, 1940 and 1980. Xs (green in web version) represent pole location and its equatorial projection, diamonds (green in web version) represent antipole location and its equatorial projection.

indeed, radial diffusion is necessary for magnetic field transport across the CMB. Furthermore, effects of radial magnetic diffusion are evident in several places on the CMB, for example, where reversed flux patches form (Gubbins, 1987; Gubbins et al., 2006; Olson and Amit, 2006). The issue here is whether radial magnetic diffusion also is responsible for the relatively large-scale structures in Fig. 5. One indication that radial diffusion is not the dominant mechanism is the change in the spatial pattern in $\dot{\rho}_e$ from one epoch to the next. Acting alone (that is, without assistance from advection by the fluid motion) it is expected that radial diffusion would result in a more stationary pattern of $\dot{\rho}_e$, rather than rapidly shifting patterns seen in Fig. 5. In fact this is a merely plausible argument against a radial diffusive origin for the $\dot{\rho}_e$ structures, certainly not a proof. Unfortunately such a proof would require measurement of the radial derivatives of the magnetic field inside the core, which we have no way of doing.

5.2. Advective mechanisms

The advective, or transport contribution to $\dot{m}_e$ involves both tangential components of the fluid velocity below the CMB and the radial field B_r on the CMB. This term is expected to play a major role in tilt changes, particularly when they are rapid. Estimating its contribution requires maps of B_r and models of the core flow at the same epochs.

In order to assess whether the time dependence of the transport term A_e is mostly due to time dependence of the magnetic field or time dependence of the core flow, we rewrite (25) as the scalar product between the tangential velocity vector $\vec{u}_h$ and a tangential kernel vector $\vec{G}$ as

$$A_e = \vec{u}_h \cdot \vec{G}, \tag{34}$$

where the azimuthal and meridional components of the kernel vector are given by

$$G_\phi = -B_r \sin\phi', \tag{35}$$

$$G_\theta = B_r \cos\theta \cos\phi'. \tag{36}$$

The azimuthal component G_ϕ amplifies the contribution from B_r at longitudes 90° away from the dipole axis. The meridional component G_θ amplifies the contribution from B_r at the longitudes of the dipole (and its antipole) and also at high latitudes. Maps of G_ϕ and G_θ are shown on the left columns of Figs. 6 and 7 for the four sampled epochs. Note that both compo-

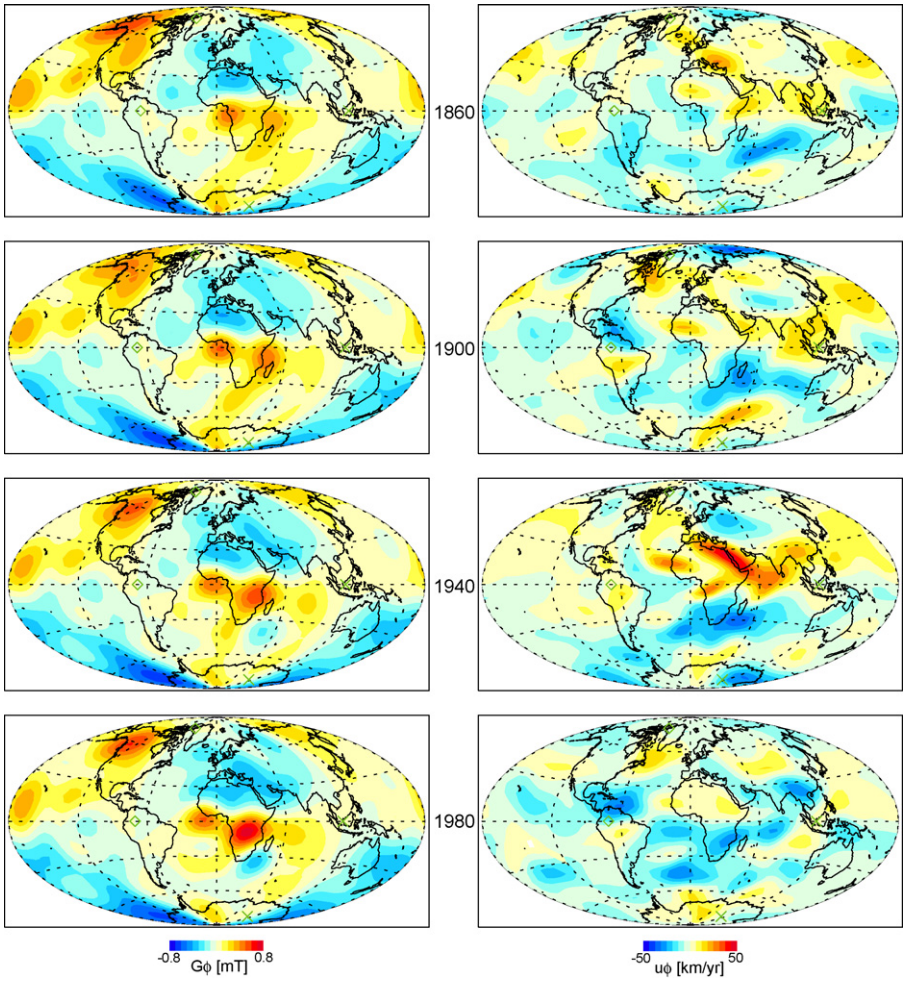

Fig. 6. Azimuthal kernel G_ϕ in mT (left) based on *gufm1* and azimuthal velocity u_ϕ in km/yr (right, black/white (red/blue in web version) denotes eastward/westward, respectively) of the frozen-flux $k = 0.15$ core flow model for 1860, 1900, 1940 and 1980.

nents of the kernel vector are rather stable, changing little over the study period. This is particularly the case for the meridional component G_θ.

Before considering complex core flows, we examine the tilt sensitivity of the core field to simple flows described by single spherical harmonic potentials of degree and order 2 or less. As expected, some of these simple flows make zero contribution to tilt change. For example, solid body rotation about the z-axis does not change m_e. Solid body rotation about an axis in the equatorial plane is very efficient in changing m_e, and such simple meridional circulation acting on a dipole field has sometimes been proposed as a mechanism for rapid tilt changes, excursions and polarity reversals (Wicht and Olson, 2004). However, such flows include cross-equator transport that tends to be suppressed by Earth's rapid rotation. They also fail on observational grounds, as they imply a large separation between the geographic and magnetic equators that is inconsistent with the structure of the present core field. We found that single harmonic toroidal core flows are more efficient at changing the tilt than single harmonic poloidal flows, by about a factor of 1.5. Moreover, considering that the toroidal component of the core flow is about an order of magnitude larger than the poloidal one (Amit and Olson, 2006), we expect toroidal flows to dominate equatorial dipole changes. Excluding the simple equator-crossing flows and poloidal flows from consideration, we are left with two simple toroidal flow candidates: $l = 2\,m = 0$ and $l = 2\,m = 1$. Substitution of these into (34)–(36) yields a large amount of cancellation over the CMB, mostly due to oppositely signed A_e structures symmetric with respect to the equator, with the non-cancelling regions limited to the reversed flux patches, and very little tilt change per unit flow amplitude. We conclude, therefore, that magnetic flux transport by simple, single harmonic core flows is unlikely to be the main cause of the observed $\dot{m}_e$.

We now consider frozen-flux core flows inferred from inversions of the geomagnetic secular variation. Numerous models of core flow have been derived by inverting the radial magnetic induction equation on the CMB assuming the frozen-flux condition is valid (e.g. Bloxham, 1989; Jackson et al., 1993; Chulliat and Hulot, 2000; Holme and Whaler, 2001; Hulot et al., 2002; Eymin and Hulot, 2005; Amit and Olson, 2006). We note that an hypothetically perfect frozen-flux representation of the core flow would satisfy the equatorial moment equation (24) exactly with D_{te} and D_{re} set to zero. In reality however, a frozen-flux core flow model will not satisfy the moment equation exactly, unless constrained to do so *a priori*. This is partly due to the fact that the secular variation spectrum on the CMB is quite

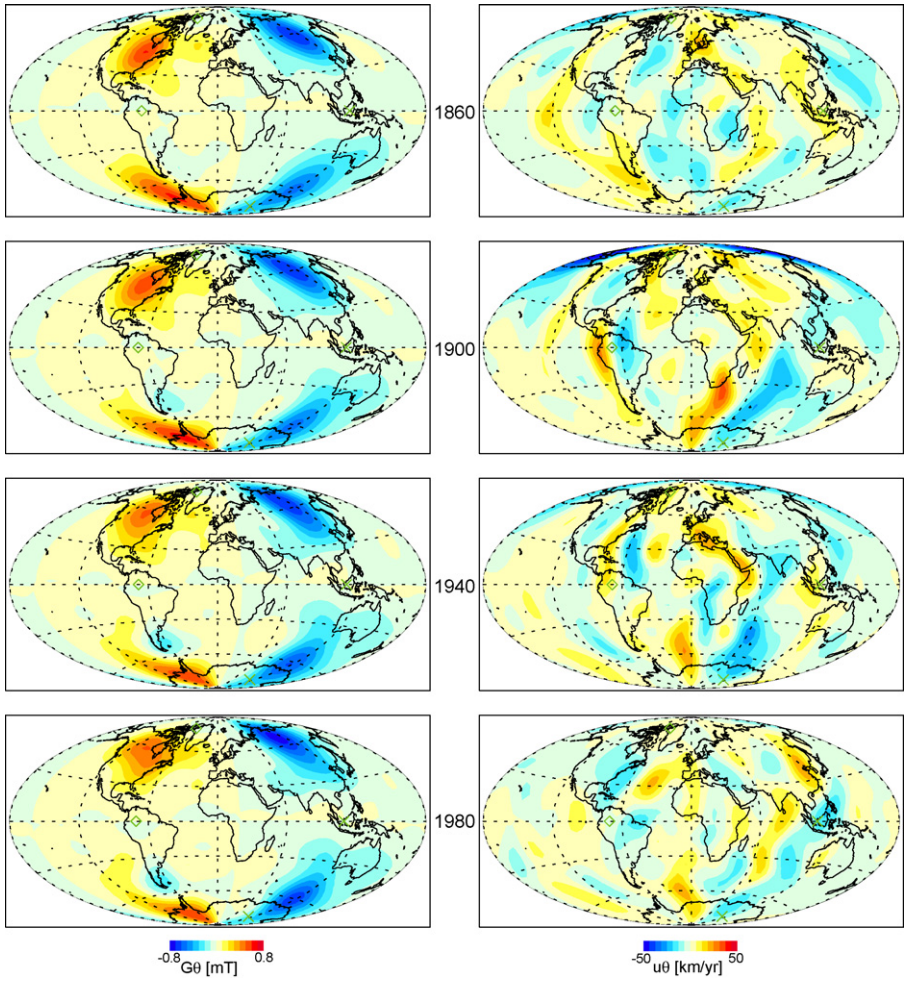

Fig. 7. Meridional kernel G_θ in mT (left) based on *gufm1* and meridional velocity u_θ in km/yr (right, black/white (red/blue in web version) denotes southward/northward, respectively) of the frozen-flux $k = 0.15$ core flow model for 1860, 1900, 1940 and 1980.

broadband, and dipolar secular variation makes up only a small portion of the total (e.g. Holme and Olsen, 2006).

Our approach uses the core flow inversion method of Amit and Olson (2004). A flow solution is obtained by inverting the frozen-flux radial magnetic induction equation just below the CMB. A finite-difference local numerical method on a regular grid is used to solve a set of two coupled differential equations for the toroidal and poloidal flow potentials. The model assumes purely helical flow for the correlation of tangential divergence and radial vorticity, with a proportionality factor k. Helical flow characterizes the relation between toroidal and poloidal flows in numerical dynamos (Olson et al., 2002; Amit et al., 2007), and it also holds in some simple rotating flows (Amit and Olson, 2004). We do not invoke any *a priori* smoothness constraints on the time continuity of the flow, and we do not apply any special weight to the dipolar secular variation. This approach does not ensure that our model fits the observed dipole moment changes. Instead it provides an unbiased image of the regions on the CMB where the advective sources and sinks of equatorial moment are concentrated, and their temporal variation. Prominent large-scale flow structures in our frozen-flux core flow solutions include a large counter-clockwise vortex in the southern hemisphere below the Indian and Atlantic Oceans, a clockwise vortex below North America, a clockwise vortex below Asia and a westward flow in the sub-equatorial part of the Atlantic southern hemisphere (Amit and Olson, 2006). Although these flow features can be identified at most snapshots throughout the 150 years period, their structure varies significantly from one epoch to another. The streamlines of the toroidal part of these flows can be seen in Fig. 8. Most frozen-flux core flow models include a similar large-scale flow pattern. Robust flow features in common to our core flow model and to other models derived using different physical assumptions such as pure toroidal flow and tangential geostrophy include the large anti-clockwise vortex below the southern Indian and Atlantic Oceans, the clockwise vortex below North America, and the westward drift at low- and mid-latitudes of the southern hemisphere (e.g. Bloxham, 1989; Jackson et al., 1993; Chulliat and Hulot, 2000; Holme and Whaler, 2001; Hulot et al., 2002; Eymin and Hulot, 2005).

How much of the equatorial dipole change can be explained by core flow advection? Our core flow model accounts for most of the amplitude and all of the trends in the observed $\dot{m}_e$ between 1840 and 1990. Fig. 9 compares the observed equatorial dipole moment change with the changes predicted by substituting our

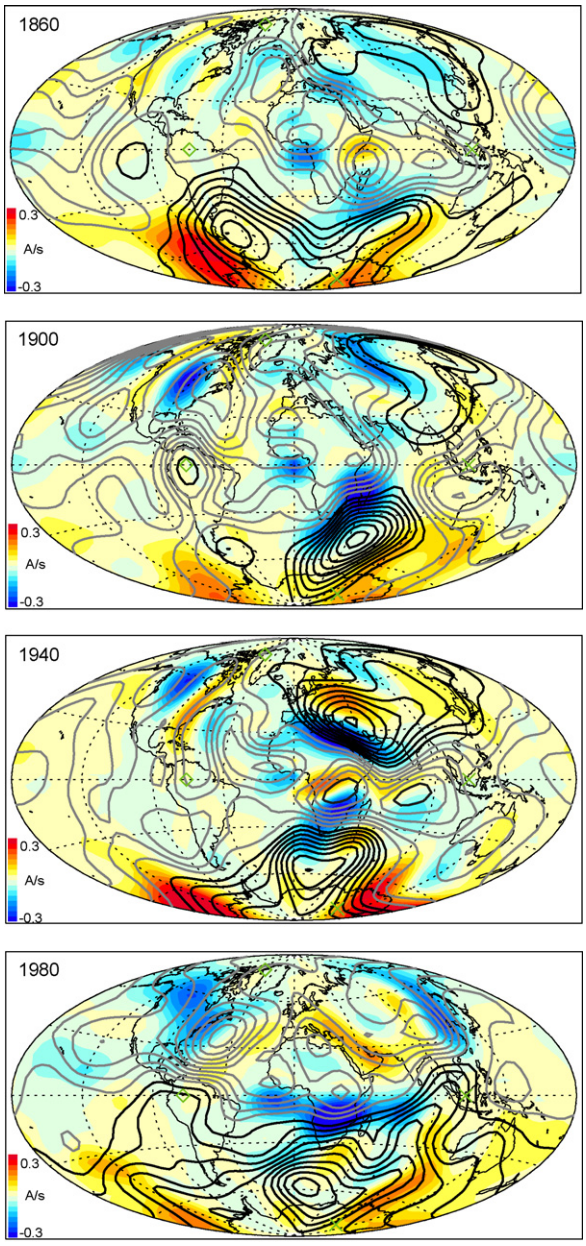

Fig. 8. Advective contributions to equatorial dipole moment change $(3/2\mu_0)A_e$ in A s^{-1} with toroidal streamlines (black/grey denotes counter-clockwise/clockwise flow) of the frozen-flux $k = 0.15$ core flow model superimposed, for 1860, 1900, 1940 and 1980. Streamline intervals are the same for all epochs, rms velocities are 8.8, 10.9, 11.1 and 9.9 km/yr, respectively.

flow models with various k values into (25). The values of $\pm 0.5T$ A m^2 s^{-1} are used arbitrarily to define the nearly constant tilt period and to distinguish it from the rapid decrease event later on. The predicted curves have similar trends and magnitudes over the entire interval, with slightly different amplitudes at different k values. The fits (rank correlations) between the observed change and the model change are 0.84, 0.85 and 0.84 for $k = 0.1$, $k = 0.15$ and $k = 0.25$, respectively. The standard deviations between the observed change and the model change are 0.41, 0.38 and 0.40 T A m^2 s^{-1}, for $k = 0.1$, $k = 0.15$ and $k = 0.25$, respectively, about one order of magnitude smaller than the observed amplitude in all cases. The best fit (largest correlation and smallest standard deviation) is obtained for the core flow model with $k = 0.15$, in agreement with the best fit for the observed length-of-day variations (Amit and Olson, 2006).

5.3. Regional sources of tilt change

Maps of A_e just below the CMB are shown in Fig. 8 at each epoch, with streamlines of our core flow model with $k = 0.15$ superimposed. Like the moment density change, these maps are spatially complex and are nearly balanced. Positive and negative A_e structures (the advective sources and sinks, respectively) vary rapidly with time and tend to cancel in any single snapshot. It is the relatively small difference between the sources and sinks integrated over the CMB that accounts for the tilt changes, even at times when the tilt change is rapid.

The origin of the A_e structures in Fig. 8 can be inferred from the distributions of $\vec{G}$ and $\vec{u}_h$ at specific times. Figs. 6 and 7 compare the azimuthal and meridional components of these two vectors. In spite of the strongly time-dependent character of A_e, flow in certain regions make particularly large contributions at most epochs. For example, the meridional limbs of the large Southern hemisphere vortex correlate with large G_θ, resulting in positive A_e structures below southeastern Pacific (where southward flow advects positive B_r away from the equatorial antipole) and below southern Indian Ocean (where northward flow advects positive B_r toward the equatorial pole). Negative A_e structures (m_e sinks) are more scattered and time variable. The most notable sink occurs where westward flow in the northern limb of the same vortex correlates with a strong G_ϕ structure below Africa. In this region positive B_r is advected away from the equatorial pole axis, producing a sink that tends to decrease m_e. Another prominent sink is located below North America, where northward meridional flow correlates with a positive G_θ structure. Here, negative B_r is advected away from the equatorial antipole to decrease m_e.

In the first three epochs shown in Fig. 8, the sources and sinks nearly cancel. This implies a small advective contribution to $\dot{m}_e$, consistent with the small observed change in m_e over this period of time (Fig. 9). The 1980 map in Fig. 8 differs from the first three epochs in this respect, for reasons that can be seen in Figs. 6 and 7. First, the tilt sink below Africa strengthened as both G_ϕ and u_ϕ intensified in this region. Second, the tilt sink below North America also strengthened, due to the broadening of the northward flow at the western limb of the vortex in that region. Finally, the two tilt sources at high latitudes in the southern hemisphere weakened somewhat, mostly because the meridional flow weakened in both regions. The net effect of these changes is a large negative $\dot{m}_e$ by advection at epoch 1980. The advective contribution to the equatorial dipole change predicted by the frozen-flux flow model shown in Fig. 8 amounts to 86% of the observed rate of equatorial dipole moment decrease at this epoch (Fig. 9), and our analysis of Figs. 6 and 7 indicates that the transition from steady to decreasing tilt involves changes in both the field and the flow, especially the latter.

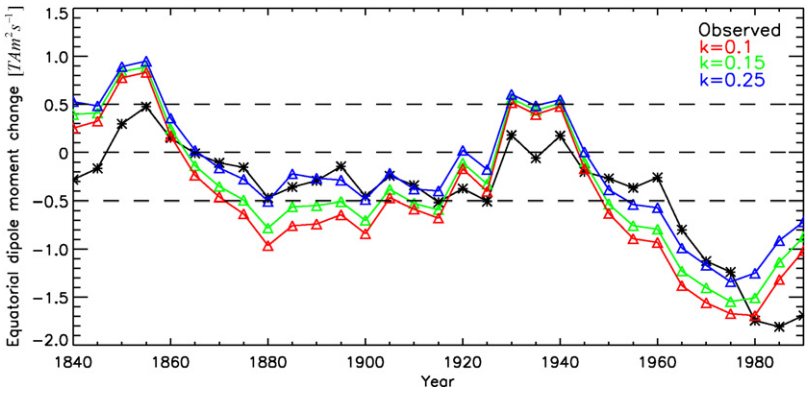

Fig. 9. Equatorial dipole moment rate of change, 1840–1990. Observed (asterisks) and frozen-flux advective contributions from core flow models (triangles) with various k values (linestyles (colors in web version), see legend). Horizontal dashed lines denote zero change and $\pm 0.5\,T\,\mathrm{A\,m^2\,s^{-1}}$ variation.

6. Tilt changes prior to 1840

Simple extrapolation of the dipole Gauss coefficients of the 2005 IGRF field model using its secular variation (Mcmillan and Maus, 2005) shows that if the current dipole secular variation persists, the dipole tilt will be less than 2° in 200 years. This scenario seems plausible, in light of the long period of equatorward motion of the dipole axis prior to 1800 (Fig. 1), in which the tilt has increased in about 7° in two centuries. It is possible that we are at the beginning of another long period of large tilt variations, this time a decrease.

Fig. 1 shows a clockwise loop motion of the dipole axis in the last four centuries with a large tilt increase prior to 1800. Because of the lack of intensity measurements prior to 1840, we do not have reliable geomagnetic secular variation data and core flow models for that period. However, it is worthwhile trying to crudely infer the kinematics of the dipole axis motion for that period by tracking geomagnetic field structures in the *gufm1* movie (Finlay and Jackson, 2003). During the long tilt increase period, the negative patch below North America moved mostly southward, approaching the equatorial antipole and increasing the tilt. In the southern hemisphere, positive magnetic flux below Patagonia has generally drifted southward away from the equatorial antipole, and positive magnetic flux below the Indian Ocean has generally drifted northward toward the equatorial pole, in both cases increasing the tilt. The positive equatorial field structures have drifted westward (away from the equatorial pole, decreasing the tilt) throughout the entire period, and the time dependency of their impact on dipole tilt change was controlled by their longitudinal distance from $\phi_0(t)$ and their drift speed. It is possible that the kinematics of the same magnetic field structures that we have identified in causing the recent tilt decrease event, the meridional motion of the negative patch below North America and the westward motion of the positive patches below Africa, have played an important role in the long period of tilt increase event prior to 1800.

Our analysis has implications for dipole behavior on longer time scales. In the *CALS7K* model, the rms azimuthal velocity is about 1.4 times larger than the rms meridional velocity. These comparable azimuthal and meridional dipole axis velocities, together with the loop-like dipole axis motion, suggest that tilt changes are equally significant as longitudinal drift in maintaining the long-term time-average geomagnetic axial dipole. In addition to periods of nearly constant tilt, the model shows several hairpin turns involving large changes in tilt, and the NGP has passed close to the geographical pole on several occasions. According to our interpretation, constant tilt corresponds to times when the magnetic field structure on the CMB is relatively stationary, apart from westward or eastward drift. Similarly, our interpretation of tilt change events is that they correspond to re-organizations of the field structure associated with and augmented by changes in the flow structure. Like the situation today, rapidly evolving magnetic field structures located far from the equatorial dipole axis can induce the abrupt changes in tilt seen in Fig. 1. It is tempting to speculate that the advective effects we have identified here may also play an important role in more sustained tilt changes, such those associated with dipole excursions and polarity reversals.

7. Summary

Since the advent of field intensity measurements, the equatorial dipole moment has been controlled by magnetic field asymmetry primarily in the southern hemisphere of the core. High-intensity magnetic flux on the core–mantle boundary beneath the southern Indian Ocean combined with weak and reversed flux beneath the South Atlantic have confined the equatorial moment vector between 108°E to 116°E longitude. We speculate that this flux asymmetry is linked to the large-scale counter-clockwise vortex in the southern hemisphere of the outer core shown in Fig. 8.

Most of the historical changes in dipole tilt can be explained by advection by large-scale core flow, in which azimuthal and meridional motions play comparably important roles. Our frozen-flux core flow models indicate that at least 84% of the historical tilt change can be accounted for this way. In certain regions, the correlation between the radial magnetic field (expressed by the kernel vector) and the fluid velocity is particularly strong, resulting in concentrated advective sources and sinks for the equatorial dipole moment.

For example, westward flux transport beneath Africa and northward flux transport beneath North America since 1960 have decreased the equatorial dipole moment by an amount that is equivalent to a reduction of the dipole tilt angle by 1.2°.

In order to account for the abrupt change in the NGP path that occurred around 1960, the large-scale core flow must be highly time variable. We find that the observed secular variation of the core field is not sufficient to explain this tilt path change if the core flow were steady. Although the main large-scale vortices seen in the core flow today can be traced back to 1840, their structure and location appear to change on time scales of several decades, according to frozen-flux models. Rapid tilt changes and abrupt NGP path changes are manifestations of this effect.

It is instructive to compare the apparent velocity of the dipole axis with typical velocities in our core flow model. The time-average azimuthal velocity of the dipole axis between 1840 and 1990 is $\dot{\phi}_0 = 0.05^\circ\ \mathrm{yr}^{-1}$ westward. This is to be compared with the $0.15^\circ\ \mathrm{yr}^{-1}$ rms zonal angular velocity of our core flow model averaged over the same time interval. The observed meridional velocity of the dipole axis at 2005 is $\dot{\theta}_0 = 0.05^\circ\ \mathrm{yr}^{-1}$ poleward. For comparison, the rms meridional angular velocity of the core flow model between 1960 and 1990 is $0.08^\circ\ \mathrm{yr}^{-1}$. The dipole axis speeds are therefore less than typical core flow speeds by a factor of 1.5–3 in each component. This difference is additional evidence that tilt changes result from perturbations to a balanced distribution of equatorial dipole sources and sinks.

An important issue we have left unresolved is the effect of radial magnetic diffusion. One interpretation of the small misfit between the observed equatorial dipole moment change and the predictions of our frozen-flux model (see Fig. 9) is that it represents the contribution from radial diffusion. However, it is also possible that this difference is simply the result of inaccuracies in our core flow model, or some combination of diffusion and model errors. Further investigation using higher resolution models of the core field may shed more light on this question.

Acknowledgments

This research was supported by a grant from the Geophysics Program of the National Science Foundation. H.A. was supported by a grant from the IntraEuropean MarieCurie Action. P.O. was supported by an NSF grant number EAR-0604974. We thank two anonymous reviewers for helpful suggestions. This is IPGP contribution 2337.

Appendix A. Contributions from magnetic diffusion to dipole moment changes

The contribution from radial magnetic diffusion to axial dipole moment change is given by

$$D_{\mathrm{r}z} = -\frac{\lambda\ \sin\theta}{r}\frac{\partial}{\partial r}(rB_\theta) \tag{A.1}$$

and the contribution from meridional magnetic diffusion is

$$D_{\mathrm{t}z} = \frac{\lambda\ \sin\theta}{r}\frac{\partial B_\mathrm{r}}{\partial\theta}. \tag{A.2}$$

The contribution from radial and tangential magnetic diffusion to $\dot{m}_x$ is respectively

$$D_{\mathrm{r}x} = \frac{\lambda}{r}\left[-\cos\theta\ \cos\phi\frac{\partial}{\partial r}(rB_\theta) + \sin\phi\frac{\partial}{\partial r}(rB_\phi)\right], \tag{A.3}$$

$$D_{\mathrm{t}x} = \frac{\lambda}{r}\left[\cos\theta\ \cos\phi\frac{\partial B_\mathrm{r}}{\partial\theta} - \frac{\sin\phi}{\sin\theta}\frac{\partial B_\mathrm{r}}{\partial\phi}\right]. \tag{A.4}$$

The contribution from radial and tangential magnetic diffusion to $\dot{m}_y$ is respectively

$$D_{\mathrm{r}y} = \frac{\lambda}{r}\left[-\cos\theta\ \sin\phi\frac{\partial}{\partial r}(rB_\theta) - \cos\phi\frac{\partial}{\partial r}(rB_\phi)\right], \tag{A.5}$$

$$D_{\mathrm{t}y} = \frac{\lambda}{r}\left[\cos\theta\ \sin\phi\frac{\partial B_\mathrm{r}}{\partial\theta} + \frac{\cos\phi}{\sin\theta}\frac{\partial B_\mathrm{r}}{\partial\phi}\right]. \tag{A.6}$$

Finally, the contribution from radial and tangential magnetic diffusion to the equatorial dipole rate of change is respectively

$$D_{\mathrm{r}e} = \frac{\lambda}{r}\left[\cos\theta\ \cos\phi'\frac{\partial}{\partial r}(rB_\theta) - \sin\phi'\frac{\partial}{\partial r}(rB_\phi)\right], \tag{A.7}$$

$$D_{\mathrm{t}e} = \frac{\lambda}{r}\left[-\cos\theta\ \cos\phi'\frac{\partial B_\mathrm{r}}{\partial\theta} + \frac{\sin\phi'}{\sin\theta}\frac{\partial B_\mathrm{r}}{\partial\phi}\right]. \tag{A.8}$$

References

Amit, H., Olson, P., 2004. Helical core flow from geomagnetic secular variation. Phys. Earth Planet. Inter. 147, 1–25.

Amit, H., Olson, P., 2006. Time-average and time-dependent parts of core flow. Phys. Earth Planet. Inter. 155, 120–139.

Amit, H., Olson, P., Christensen, U., 2007. Tests of core flow imaging methods with numerical dynamos. Geophys. J. Int. 168, 27–39.

Bloxham, J., 1989. Simple models of fluid-flow at the core surface derived from geomagnetic-field models. Geophys. J. Int. 99, 173–182.

Bloxham, J., 2002. Time-independent and time-dependent behaviour of high-latitude flux bundles at the core–mantle boundary. Geophys. Res. Lett. 29, 1854.

Bloxham, J., Gubbins, D., 1985. The secular variation of the Earth's magnetic field. Nature 317, 777–781.

Brasseur, G., Solomon, S., 1984. Aeronomy of the Middle Atmosphere. Reidel, Boston.

Bullard, E.C., Freedman, C., Gellman, H., Nixon, J., 1950. The westward drift of the Earth's magnetic field. Philos. Trans. R. Soc. Lond. A 243, 67–92.

Carlut, J., Courtillot, V., Hulot, G., 2000. Over how much time should the geomagnetic field be averaged to obtain the mean paleomagnetic field? Terra Nova 11, 39–243.

Christensen, U., 2006. A deep dynamo generating Mercury's magnetic field. Nature 444, 1056–1058.

Chulliat, A., Hulot, G., 2000. Local computation of the geostrophic pressure at the top of the core. Phys. Earth Planet. Inter. 117, 309–328.

Connerney, J.E.P., Acuna, M.H., Ness, N.F., 1987. The magnetic field of Uranus. J. Geophys. Res. 92, 15329–15336.

Connerney, J.E.P., Acuna, M.H., Ness, N.F., 1992. The magnetic field of Neptune. Adv. Space Res. 12, 239–248.

Davidson, P.A., 2001. An Introduction to Magnetohydrodynamics. Cambridge University Press, Cambridge, p. 173.

Eymin, C., Hulot, G., 2005. On large and small-scale core surface flows inferred from magnetic satellite data. Phys. Earth Planet. Inter. 152, 200–220.

Finlay, C.C., Jackson, A., 2003. Equatorially dominated magnetic field changes at the surface of Earth's core. Science 300, 2084–2086.

Gubbins, D., 1987. Mechanisms of geomagnetic polarity reversals. Nature 326, 167–169.

Gubbins, D., Bloxham, J., 1987. Morphology of the geomagnetic-field and implications for the geodynamo. Nature 325, 509–511.

Gubbins, D., Jones, A.L., Finlay, C.C., 2006. Fall in Earth's magnetic field is erratic. Science 312, 900–902.

Heimpel, M., Aurnou, J., Wicht, J., 2005. Simulation of equatorial and high-latitude jets on Jupiter in a deep convection model. Nature 438, 193–196.

Heirtzler, J.R., 2002. The future of the South Atlantic anomaly and implications for radiation damage in space. J. Atmos. Solar Terr. Phys. 64, 1701–1708.

Hide, R., 1966. Free hydromagnetic oscillations of the Earth's core and the theory of the geomagnetic secular variation. Philos. Trans. R. Soc. Lond. A 259, 615–650.

Holme, R., Olsen, N., 2006. Core surface flow modelling from high resolution secular variation. Geophys. J. Int. 166, 518–528.

Holme, R., Whaler, K.A., 2001. Steady core flow in an azimuthally drifting reference frame. Geophys. J. Int. 145, 560–569.

Hongre, L., Hulot, G., Khokhlov, A., 1998. An analysis of the geomagnetic field over the past 2000 years. Phys. Earth Planet. Sci. 106, 311–335.

Hulot, G., Eymin, C., Langlais, B., Mandea, M., Olsen, N., 2002. Small-scale structure of the geodynamo inferred from Oersted and Magsat satellite data. Nature 416, 620–623.

Jackson, A., Bloxham, J., Gubbins, D., 1993. Time-dependent flow at the core surface and conservation of angular momentum in the coupled core–mantle system. In: LeMouël, J.-L., Smylie, D.E., Herring, T. (Eds.), Dynamics of Earth's deep interior and Earth rotation. Geophys. Monogr. Ser., 72, pp. 97–107.

Jackson, A., Jonkers, A.R.T., Walker, M.R., 2000. Four centuries of geomagnetic secular variation from historical records. Philos. Trans. R. Soc. Lond. 358, 957–990.

Keiling, A., Wygant, J.R., Cattell, C.A., Mozer, F.S., Russell, C.T., 2003. The global morphology of wave Poynting flux: powering the aurora. Science 299, 383–386.

Korte, M., Constable, C.G., 2005. Continuous geomagnetic field models for the past 7 millenia. 2. CALS7K. Geochem. Geophys. Geosyst. 6, Q02H16.

McFadden, P.L., Merrill, R.T., McElhinny, M.W., 1985. Non-linear processes in the geodynamo: paleomagnetic evidence. Geophys. J. Roy. Astron. Soc. 83, 111–126.

Mcmillan, S., Maus, S., 2005. International geomagnetic reference field—the tenth generation. Earth Planets Space 57, 1135–1140.

Merrill, R.T., McElhinny, M.W., McFadden, P.L., 1998. The Magnetic Field of the Earth: Paleomagnetism, The Core, and The Deep Mantle. Academic Press, San Diego.

Merrill, R.T., McFadden, P.L., 1999. Geomagnetic polarity transitions. Rev. Geophys. 37, 201–226.

Moffatt, H.K., 1978. Magnetic field generation in electrically conducting fluids. Cambridge University Press, Cambridge, p. 111.

Newell, P., Meng, C.-I., 1989. Dipole tilt effects on the latitude of the cusp and cleft/low-latitude boundary layer. J. Geophys. Res. 94, 6949–6953.

Olsen, N., Luhr, H., Sabaka, T.J., Mandea, M., Rother, M., Tøffner-Clausen, L., Choi, S., 2006. CHAOS—a model of the Earth's magnetic field derived from CHAMP, Ørsted, and SAC-C magnetic satellite data. Geophys. J. Int. 166, 67–75.

Olson, P., Amit, H., 2006. Earth's changing dipole. Naturwissenschaften 93 (11), 519–542.

Olson, P., Sumita, I., Aurnou, J., 2002. Diffusive magnetic images of upwelling patterns in the core. J. Geophys. Res. 107.

Østgaard, N., Mende, S.B., Frey, H.U., Sigwarth, J.B., Asnes, A., Weygand, J.M., 2007. Auroral conjugacy studies based on global imaging. J. Atmos. Solar Terr. Phys. 69, 249–255.

Russell, C.T., Yu, Z.J., Khurana, K.K., Kivelson, M.G., 2001. Magnetic field changes in the inner magnetosphere of Jupiter. Adv. Space Res. 28, 897–902.

Smith, E.J., Davis, L., Jones, D.E., Coleman, P.J., Colburn, D.S., Dyal, P., Sonett Jr., C.P., 1975. Jupiter's magnetic field. Magnetosphere, and interaction with the solar wind: Pioneer 11. Science 188, 451–455.

Smith, E.J., Davis, L., Jones, D.E., Coleman, P.J., Colburn, D.S., Dyal, P., Sonett Jr., C.P., 1980. Saturn's magnetic field and magnetosphere. Science 207, 407–410.

Stanley, S., Bloxham, J., 2004. Convective-region Geometry as the Cause of Uranus' and Neptune's Unusual Magnetic Fields.

Stevenson, D.J., 1980. Saturn's luminosity and magnetism. Science 208, 746–748.

Wicht, J., Olson, P., 2004. A detailed study of the polarity reversal mechanism in a numerical dynamo model. Geochem. Geophys. Geosyst. 5.

Yukutake, T., 1967. The westward drift of the Earth's magnetic field in historic times. J. Geomag. Geoelect. 23, 11–23.